Thin Solid Films 545 (2013) 279–284

Contents lists available at ScienceDirect

Thin Solid Films

journal homepage: www.elsevier.com/locate/tsf

Structural, morphological, optical and photoluminescence properties of HfO_2 thin films

C.Y. Ma *, W.J. Wang, J. Wang, C.Y. Miao, S.L. Li, Q.Y. Zhang

Key Laboratory of Materials Modification by Laser, Ion and Electron Beams, Dalian University of Technology, Ministry of Education, Dalian 116024, China

ARTICLE INFO

Article history:
Received 18 July 2012
Received in revised form 13 August 2013
Accepted 15 August 2013
Available online 26 August 2013

Keywords:
Hafnium dioxide
Sputtering
Optical Properties
Luminescence

ABSTRACT

Nanocrystalline monoclinic HfO_2 films with an average crystal size of 4.2–14.8 nm were sputter deposited under controlled temperatures and their structural characteristics and optical and photoluminescence properties have been evaluated. Structural investigations indicate that monoclinic HfO_2 films grown at higher temperatures above 400 °C are highly oriented along the (−111) direction. The lattice expansion increases with diminishing HfO_2 crystalline size below 6.8 nm while maximum lattice expansion occurs with highly oriented monoclinic HfO_2 of crystalline size about 14.8 nm. The analysis of atomic force microscopy shows that the film growth at 600 °C can be attributed to the surface-diffusion-dominated growth. The intensity of the shoulderlike band that initiates at ~5.7 eV and saturates at 5.94 eV shows continued increase with increasing crystalline size, which is intrinsic to nanocrystalline monoclinic HfO_2 films. Optical band gap varies in the range 5.40 ± 0.03–5.60 ± 0.03 eV and is slightly decreased with the increase in crystalline size. The luminescence band at 4.0 eV of HfO_2 films grown at room temperature can be ascribed to the vibronic transition of excited OH^* radical while the emission at 3.2–3.3 eV for the films grown at all temperatures was attributed to the radiative recombination at impurity and/or defect centers.

1. Introduction

Hafnium dioxide (HfO_2) is a wide band gap, high dielectric constant, and high refractive index insulator with good thermal stability. On the basis of these properties, thin film HfO_2 has been investigated for use in the field of electronics, magnetoelectronics, structural ceramics, and optoelectronics [1,2]. HfO_2 has been identified as one of the most promising materials for high-*k* replacement of SiO_2 in the next generation of complementary metal-oxide-semiconductor devices [3]. These interesting applications have led to numerous efforts to synthesize HfO_2 films by various techniques, including chemical vapor deposition [4], sol–gel process [5], pulsed laser deposition [6], electron beam evaporation and sputtering [7,8], among them, reactive sputtering being one of the most widely used.

In the sputtering technique, controlled growth and manipulation of specific crystal structures at the nanoscale dimensions have important implications for the applications of HfO_2. However, it is well known that the film's optical and electronic properties, which are essentially affected by the structural defects or trap centers in hafnia [9,10], are highly dependent on the structural characteristics (i.e., structure, crystallite size, crystallographic texture and morphology) and chemistry, which is in turn controlled by the fabrication technique, growth conditions and post-deposition processes etc. From the viewpoint described above, the ability to tailor the properties so as to optimize performance requires a detailed understanding of the structural characteristics and optical and electronic properties of nanocrystalline HfO_2 films. One approach to investigate defect energy levels in HfO_2 films is using photoluminescence (PL) spectroscopy. Several emission bands of HfO_2 in the photo energy range of 2–4.5 eV have been noticed. Ito et al. [11] used PL to study HfO_2 films synthesized with various methods. They found that HfO_2 films have similar PL characteristics regardless of preparation methods. Ni et al. [12] showed two broad bands in the visible range of the PL emission spectra of HfO_2 films which were due to oxygen vacancies involved during deposition. The intensity of the PL absorptions can be either enhanced by annealing in argon or diminished by annealing in oxygen. Kiisk et al. further investigated the intensity of PL emission of HfO_2 increased due to its defects and self-trapped excitions [13]. Interestingly, markedly different results have been obtained depending on growth conditions indicating the complexity of the defect state in HfO_2 films. In this paper, we report our experimental results on the structural characteristics, optical properties and PL features of nanocrystalline HfO_2 films grown at various conditions by RF reactive sputtering. The correlation between structural characteristics and optical and PL properties was systematically studied with x-ray diffraction (XRD), atomic force microscopy (AFM), UV/VIS spectrophotometry, and PL measurements.

* Corresponding author.
E-mail address: chunyuma@dlut.edu.cn (C.Y. Ma).

0040-6090/$ – see front matter © 2013 Elsevier B.V. All rights reserved.
http://dx.doi.org/10.1016/j.tsf.2013.08.068

2. Experimental details

Hafnium oxide films were deposited by radio frequency magnetron sputtering from a metallic hafnium target with a diameter of 60 mm. Fused SiO_2 substrates and n-type-doped Si (001) wafers were used as substrates. All the substrates were ultrasonically cleaned in acetone and ethanol for 10 min. Silicon wafers were precleaned with a dilute HF solution to remove the native oxide. The vacuum chamber was evacuated to 8.5×10^{-4} Pa using a turbomolecular pump. The used sputtering gas (Ar) and the reactive gas (O_2) were 99.999% pure and introduced into the chamber by separate inlets and controlled by standard mass flow controllers. Deposition was carried out at 0.5 Pa in ambient mixtures of Ar at 30 SCCM (standard-state cubic centimeter minute) and O_2 at 5 SCCM. The RF sputtering power during growth was maintained at 120 W with an average reflected power of about 0 W. The substrate temperature during deposition was monitored using a chromel-alumel thermocouple close to the top of the substrates. A heater mounted above the holder enables the temperature of the substrate to be varied from room temperature (RT) to 800 °C. The films studied in this work were 125–165 nm in thickness and they were grown at the substrate temperatures of RT (28–47 °C), 200 °C, 400 °C and 600 °C for 2 h.

Phase structure and growth orientations of the films were analyzed by XRD using unresolved Cu $K\alpha$ radiation (wavelength $\lambda_{x\text{-}ray} = 0.1542$ nm, D/Max 2400). A typical 2θ scan in the range of 25–80° and a step size of 0.02° were employed. AFM on a CSPM5500 scanning probe microscope was used in contact mode with a scan frequency of 1.0 Hz to measure the surface morphologies and roughness of the films. The measurement of transmittance (T) and reflectance (R) at normal incidence of the films deposited on the fused SiO_2 substrate was performed in the wavelength range of 190–1100 nm using a Lambda-35 UV/VIS spectrometer. PL spectra were recorded by using a Fluorescence spectrometer (Edinburgh Instr.Model-FLS920) with a 450 W Xenon lamp as excitation source and excitation and emission of 3.0 nm slit width.

3. Results and discussion

3.1. Structural characterization

The XRD patterns obtained in the HfO_2 films grown at temperatures from RT to 600 °C are shown in Fig. 1. The XRD curve of HfO_2 grown at RT indicates the polycrystalline nature of the samples. The peaks can be unambiguously assigned to monoclinic HfO_2 as labeled in Fig. 1 (referenced JCPDS 74–1506). The peak at the 2θ angle of ~28.3° corresponding to (−111) orientation is seen to be very broad indicating the presence of very small nanoparticles. It is evident that the x-ray peak intensity at 28.3° increases with increasing growth temperature of HfO_2. At temperatures of 400 °C, crystalline with (−111) planes oriented parallel to the substrate preferentially formed, although minor peaks due to other orientations of monoclinic crystallites were also present. The XRD curve of HfO_2 films grown at 600 °C indicates their well and highly oriented nature. This is an indicative of an increase in average crystalline size and preferred orientation along (−111). The (−111) planes are the lowest surface energy in monoclinic HfO_2. Crystallites with (−111) planes oriented perpendicular to the growth direction in a film therefore represent the lowest energy orientation and are thermodynamically preferred.

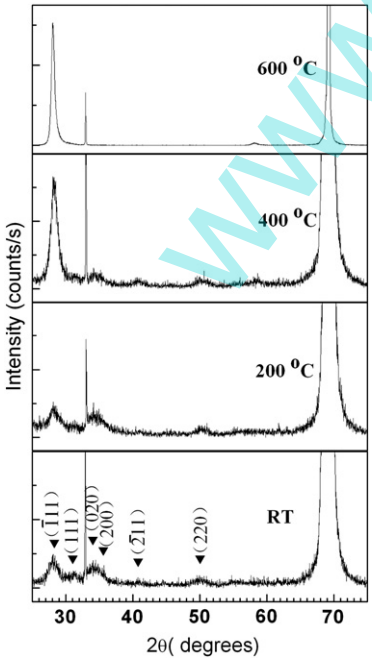

Fig. 1. XRD patterns from samples grown at different substrate temperatures.

Scans of the (−111) peak are shown in Fig. 2(a). A shift to the higher angle with increasing temperatures from RT to 400 °C can be noted. Further increasing to 600 °C results in the shift of the (−111) peak position to a lower angle. The average grain size was estimated according to the Scherrer equation from the full width at half maximum of the −111 reflection peak, which was obtained by fitting the curve by Gaussian shaped lines. Fig. 2. (b) shows the d spacing (d_{-111}) and grain size for HfO_2 films. The grain size becomes larger with the increasing temperature. The mean grain size is 4.2 nm, 5.1 nm, 6.8 nm, and 14.8 nm for HfO_2 films grown at RT, 200 °C, 400 °C, and 600 °C respectively. It is important to recognize that d spacing (d_{-111}) decreases with an increasing grain size of below 6.8 nm, but becomes larger with a grain size of 14.8 nm. The lattice expansion occurs with decreasing crystalline size in smaller crystalline sizes, while it becomes obvious in larger crystalline sizes with preferred orientation. The well-oriented structure associated with the surface-diffusion-dominated growth, observed in XRD data coupled with AFM images for HfO_2 films grown at 600 °C indicates that

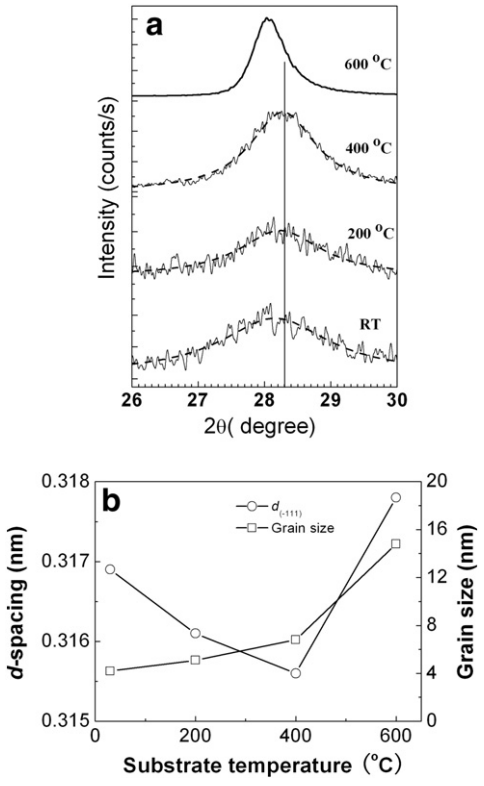

Fig. 2. (a) XRD scans of monoclinic (−111) peaks of HfO_2 films from samples grown at different substrate temperatures. (b) Variation in d spacing and average grain size for HfO_2 films.

the situation is entirely different as compared to films grown at RT-400 °C. The strain induced in the (−111) preferred orientation of the film grown at 600 °C may be the main reason for the lattice expansion in the larger crystallites. On the other hand, for small crystallines such as below 10 nm, lattice expansion in ionic solids can be attributed to other causes including a reduction in cation charge state and repulsion of strong surface dipoles leading to a reduction in surface tension. In the present case, because Hf forms cations with only a single charge state +2 surface dipole repulsion causes the lattice expansion in small crystallines observed here.

3.2. Surface morphology and scaling analysis

Fig. 3. shows large-scale ($2 \times 2\ \mu m^2$) AFM images of HfO_2 thin films grown at RT, 200 °C, 400 °C and 600 °C, respectively. There are two patterns seen in the lumps. The first is where the surface height (peak to valley) decreases with increased substrate temperature. The second is where the lateral size of the film grown at 600 °C is markedly smaller than that of the films grown at temperatures from RT to 400 °C. The surface morphology has an irregular geometry with a self-affine structure determined by the thermodynamic environment. Power spectral density analysis has been widely used for quantitative surface characterizations with spatial resolution of the roughness and correlations between roughness and specific surface features. We analyze the scaling behavior of the surface AFM topological profile using the one-dimensional power spectral density (1DPSD) [14,15].

$$1\mathrm{DPSD}(f) = \frac{1}{L}\left|\int_0^L y(x)e^{i2\pi fx}dx\right|^2 \quad (1)$$

where $y(x)$ is the topographical profile, L is the scan length, f is the spatial frequency, and x is the fast scan direction of the image.

The log–log 1DPSD plots of AFM topographical morphologies corresponding to Fig. 3 as a function of T_s are presented in Fig. 4. The 1DPSD plots exhibit frequency-independent roughness at low frequencies (long length scale), with a frequency-dependent (constant slope) 1DPSD magnitude at smaller length scales indicating self-similar roughness at these higher frequencies. By fitting the 1DPSD plots with the power law decay of 1DPSD $(f) = K_0 f^{-\gamma}$ over the frequency range, we obtained values for $-\gamma_1$, $-\gamma_2$ and $-\gamma_3$ for HfO_2 thin films. As shown in Fig. 4, HfO_2 thin films grown at below 600 °C have two separate regions of self-similar constant slope PSD behavior. Three slopes $-\gamma_1$, $-\gamma_2$ and $-\gamma_3$ were clearly observed. The dependence can be fitted by the $f^{-\gamma_3}$ and $f^{-\gamma_2}$ power law decays at high and intermediate frequencies, respectively. The magnitude of γ_2 and γ_3 is dependent on growth conditions, and γ_1 is equals to zero at low frequencies.

According to the scaling theory, the appearance of an intermediate region ($-\gamma_2$) indicates a new coarsening mechanism, such as the shadowing effect and/or grain growth effect. Surface diffusion dominated growth leads to a smooth and even film surface, while grain growth and shadowing effects cause a rough surface morphology. The competition between these effects determines the final surface morphology of the film. The 1DPSD plots have the same form for HfO_2 thin films grown at RT-400 °C, indicating a generally similar coarsening mechanism in these cases. As listed in Table 1, the high frequency slopes for HfO_2 films grown at RT-400 °C increases from −3.38 to −3.81 with increasing T_s, near to that characterizing the surface diffusion dominated film growth ($-\gamma_3 \approx -4$). For the HfO_2 thin film grown at 600 °C, the intermediate region with a slope of $-\gamma_2$ disappeared, and the dependence at high frequency can be fitted by the $f^{-3.9}$ power law decay, indicating that the surface diffusion effect was properly improved. The R_{RMS} value shows a relative smooth surface, suggesting a surface diffusion dominated smoothing mechanism. In addition, the correlation length (L_C) of a self-affine structure, which is the range corresponding to the intersection between the self-affine branch and the plateau, is determined by

$$\xi = \exp\left\{\frac{\ln(1\mathrm{DPSD}(1/L) - \ln K_0}{\gamma}\right\} \quad (2)$$

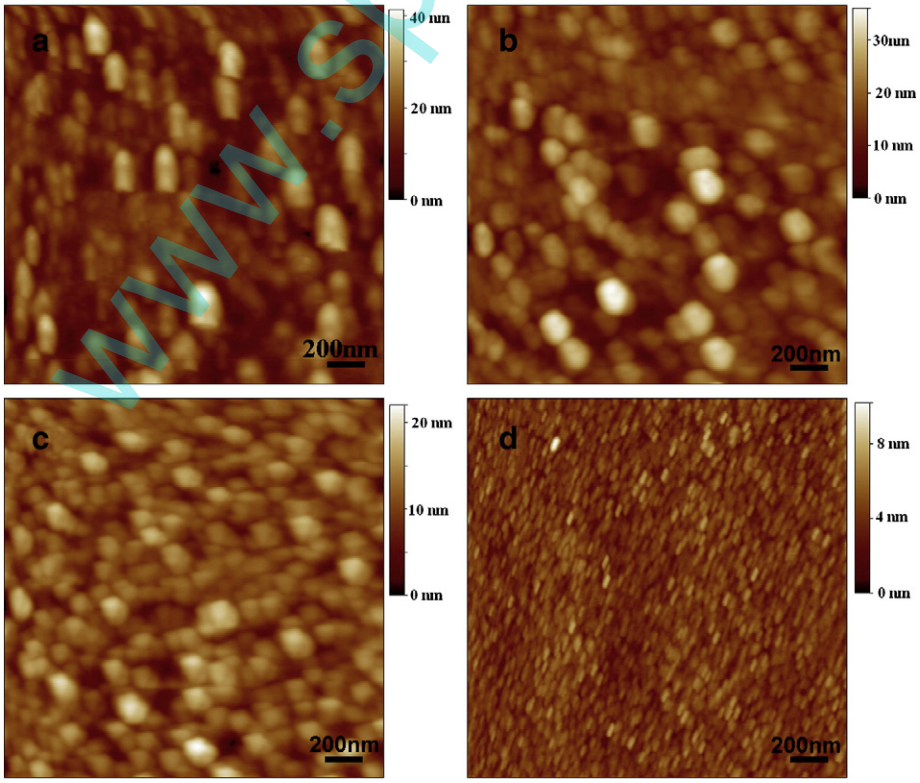

Fig. 3. AFM surface morphologies of HfO_2 films (a) RT, (b) 200 °C, (c) 400 °C, and (d) 600 °C.

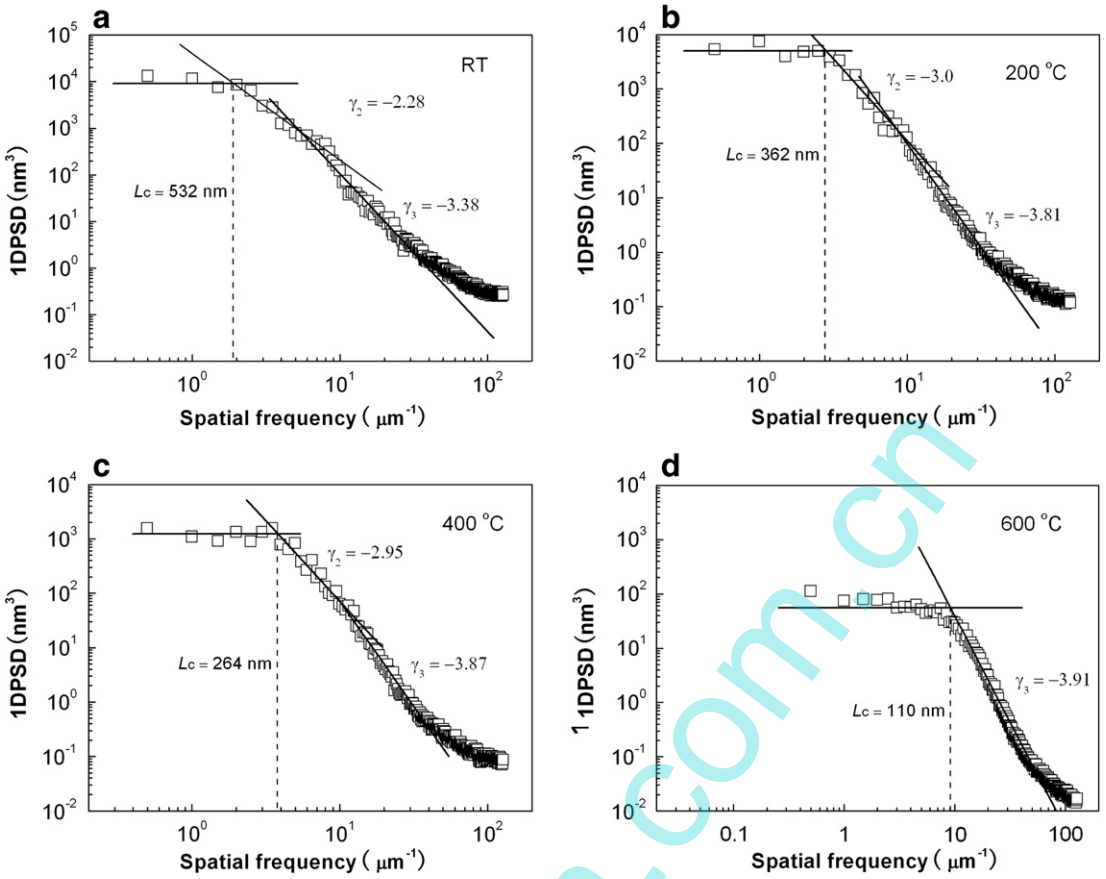

Fig. 4. 1DPSD spectra of HfO_2 films grown at (a) RT, (b) 200 °C, (c) 400 °C, and (d) 600 °C.

where K_0 is a constant. The low-frequency plateau 1DPSD ($1/L$) is related to the saturation roughness, which represents the lack of the local association on the low frequency. Therefore L_C values can define the mean lateral extension of a surface feature stable against surface diffusion. The L_C values decrease with increasing substrate temperature and are listed in Table 1, which has a relationship with the effective radius of the domain and film thicknesses.

3.3. Optical characterization

For HfO_2 films grown at various temperatures, transmittance spectra (not shown) exhibit very high transparency in the spectral region except where the incident radiation is absorbed across the band gap (E_g). This observation indicates the high quality and transparent nature of HfO_2 films with an absorption coefficient less than 1 μm^{-1} when $\lambda \geq 250$ nm. For polycrystalline thin films, light scattering caused by surface roughness and grain boundaries should also be considered for accurate evaluation of absorption coefficients. For instance, at the photon energy of 2.56 eV, i.e. in the transparency range, due to light scattering at the film surface and grain boundaries we obtained absorption coefficients of 0.49 μm^{-1}, 0.21 μm^{-1}, 0.18 μm^{-1} and 0.1 μm^{-1} for the HfO_2 deposited at RT, 200 °C, 400 °C, and 600 °C, respectively, which are consistent with our results of surface roughnesses and grain sizes described above. Fig. 5 shows α(E) versus E data. The optical absorption coefficient of the HfO_2 films is evaluated using the relation:

$$\alpha = \frac{1}{t} \ln\left[\frac{T}{(1-R)^2}\right] \quad (3)$$

where T is the transmittance, R is the reflection, and t is the film thickness. Eq. (3) is valid in the region of α(E), where the effect of

Table 1
Values from 1DPSD analysis of surface morphology for HfO_2 films.

	R_{RMS} (nm)	L_C (nm)	γ_2	γ_3
RT	4.88	532	−2.28	−3.38
200 °C	4.82	362	−3.0	−3.81
400 °C	2.66	264	−2.95	−3.87
600 °C	0.86	110	–	−3.91

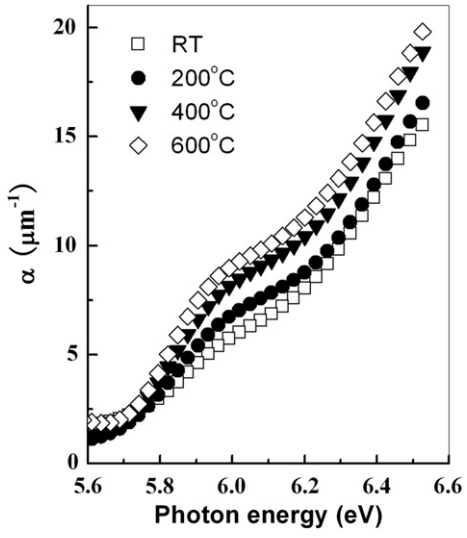

Fig. 5. Absorption spectra of HfO_2 films grown at different substrate temperatures.

multiple reflections on the magnitude of the transmitted beam is negligible. It can be seen that α(E) rises rapidly above E = 6.2 eV for all films. This feature is independent of the crystallite size. The rapid rise in α(E) for E ≥ 6.2 eV is associated with O 2*p* → Hf 5*d* interband electron transitions between Γ → B points on the reciprocal lattice of monoclinic HfO_2.

In contrast, there is a large difference in the α(E) vs E curves below 6.2 eV of HfO_2 films grown at different temperatures. A band that initiates at ~5.7 eV and saturates at 5.94 eV appears as a low energy shoulder on the absorption edge of the films at RT and develops into a discrete and more intense feature upon increasing substrate temperatures. The band's spectral position is unaffected by increasing crystalline size. However, the band's maximum intensity shows continued increase with increasing crystalline size. Note that the films grown at low substrate temperatures (RT and 200 °C) are nanocrystalline monoclinic and the films grown at high substrate temperatures (400 °C and 600 °C) are well-crystallined monoclinic with a strong (−111) texture. Comparing the shoulderlike feature with the XRD and AFM results, there is a direct correlation between the crystallization of HfO_2 films with the shoulderlike feature. We conclude that the strength of the band depends on the volume of material in which the Hf:O coordination is the same as that in bulk HfO_2. This is consistent with its cause being intrinsic to crystalline hafnium oxide rather than the defect states. The shoulderlike feature was addressed by several other investigators. Bharathi et al. [16] observed the feature on their α(E) ∝ E spectra that are very similar to that of our films and proposed that it is related to the formation of self-trapped excitions. Nguyen et al. [17] also reported an $\alpha(E)^{1/2} \propto E$ spectrum that is very similar to that of our films and that of Bharathi. They suggested that the shoulder was not caused by interband transitions but by unspecified localized states 0.2–0.3 eV below the Hf 5*d* electron band that are present only in crystalline materials.

In the E_g region (high absorption) or above the fundamental absorption edge, the absorption follows a power law in the form of

$$(\alpha h\nu) = B\left(h\nu - E_g\right)^2 \tag{4}$$

where hν(E) is the energy of the incident photon, B is the absorption edge width parameter, and E_g is the band gap. The $(\alpha h\nu)^{1/2}$ versus E plots for HfO_2 films are shown in Fig. 6. The linear fit of the data indicates the characteristic feature of HfO_2 with an indirect band gap. We obtained indirect band gap energies of 5.60 ± 0.03, 5.47 ± 0.03, 5.44 ± 0.03, and 5.40 ± 0.03 eV, respectively, for the films deposited at RT, 200 °C, 400 °C, and 600 °C. The value of the band gap for our films is in good agreement with the literature values for HfO_2 films grown by many techniques.

3.4. Photoluminescence characterization

Photoluminescence is a very sensitive and effective tool for the investigation of the electron structure of defect centers. It reflects the presence of the localized states in a band gap. The method has also been used to investigate the electron structure of HfO_2 films. Fig. 7 shows the PL spectra of HfO_2 thin films grown at various temperatures. The excitation of HfO_2 films grown at RT with a photon energy of 4.6 eV leads to an emission spectrum consisting of two wide emission bands with maxima at 3.2 eV (388 nm) and 4.0 eV (310 nm). The films grown at 200–600 °C only showed a dominating emission band at 3.2–3.3 eV (376–388 nm). Contrary to the emission band located at 3.2 eV of the films grown at 600 °C, a steady enhancement (about 2–4 times) of the emission band of the films grown at 200–400 °C was observed. The results presented in Fig. 7 show that the film grown at RT possesses different

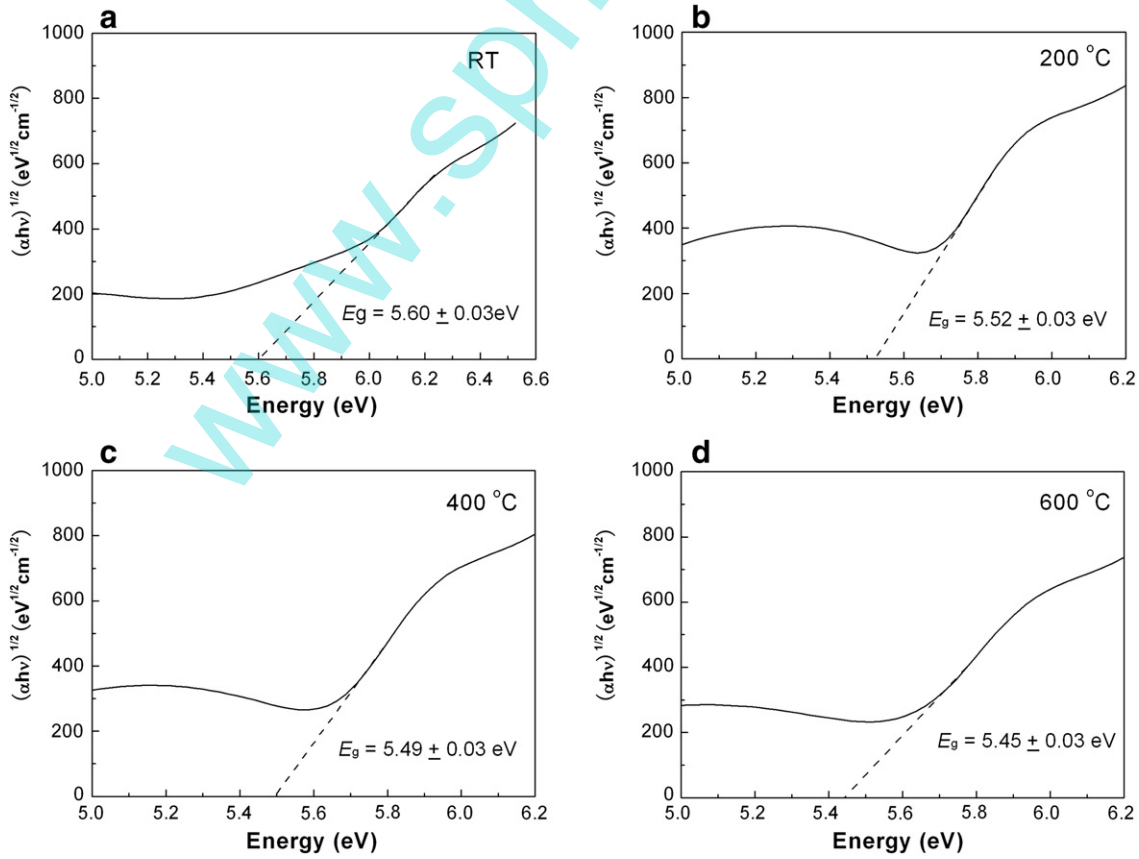

Fig. 6. Plots of the $(\alpha h\nu)^{1/2}$ vs hν curve for HfO_2 films grown at (a) RT, (b) 200 °C, (c) 400 °C, and (d) 600 °C.

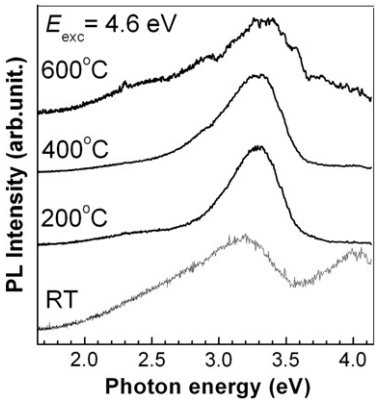

Fig. 7. Photoluminescence emission spectra for HfO_2 films grown at RT, 200 °C, 400 °C, and 600 °C. The excitation energy is 4.6 eV.

photoluminescence characteristics compared with other samples grown at 200–600 °C. In the film grown at RT, the emission band at peak energy of 4.0 eV can be ascribed to the vibronic transition of excited OH^* radical via $A^2\Sigma^+ \leftrightarrow X^2\Pi$. Similar PL observation for HfO_2 thin films deposited with the chemical vapor deposition method was reported by Rastorguev et al. [18]. We believe that the appearance of the emission band is most likely due to the presence of H_2O molecules and OH groups containing films. At low substrate temperatures, water easily enters into the films during the film deposition. In HfO_2 films, 4.6 eV photon excitation is enough for generating OH^* radicals for H_2O molecules.

The emission band at the peak energy of 3.2–3.3 eV of the films grown at all temperatures has probably an extrinsic origin arising from the radiative recombination at impurity and/or defect centers. Recombination of photo-excited electron–hole pairs captured by those centers leads to emission. Ciapponi et al. [19] reported that the photoluminescence spectra of HfO_2 thin films deposited by electron beam deposition using a metallic hafnium target are closely related to film thicknesses and stress. Thin samples with a compressive strain show a relatively weak luminescence, which is agreement with the PL spectrum in our HfO_2 films grown at elevated temperatures. In addition, the smaller crystalline size of films grown at 200-400 °C compared with those of films grown at 600 °C might be a reason for the higher concentration of defects. Besides formation of defects inside crystallites, relatively small crystalline sizes and significant contribution of interfaces between crystallites can be proposed as possible reasons for the defective nature of these films. Further studies are needed to clarify what kind of defects and/or impurities most significantly influence the PL properties of HfO_2 films.

4. Conclusion

This study reports the significant effect of substrate temperature on the structural, optical and PL properties of sputtered HfO_2 films. The XRD patterns reveal that all HfO_2 films show a monoclinic phase with nanocrystalline structure. The films grown at elevated temperatures are highly oriented along the (−111) direction. The lattice expansion increases with diminishing HfO_2 of crystalline size below 6.8 nm while maximum lattice expansion occurs with highly oriented monoclinic HfO_2 of crystalline size about 14.8 nm. Quantitative surface characterization for the films grown at different substrate temperatures by 1DPSD analysis shows that the film growth at 600 °C can be attributed to the surface-diffusion-dominated growth. Energy band gap energies of 5.60 ± 0.03, 5.47 ± 0.03, 5.44 ± 0.03, and 5.40 ± 0.03 eV are obtained for the films grown at RT, 200 °C, 400 °C, and 600 °C respectively. The PL spectra reveal that the emission at 3.2–3.3 eV for the films grown at all temperatures can be attributed to the radiative recombination at impurity and/or defect centers. The results as presented here in this paper provide a relationship between the structural characteristics and optical and PL properties of nanocrystalline HfO_2 films and could be useful to optimize the conditions while considering their potential technological applications.

Acknowledgments

The work is supported by the National Natural Science Foundation of China under grant nos. 10605009 and 10774018 and Fundamental Research Funds for the Central Universities no. DUT11LK44.

References

[1] L. Armelo, H. Bertagnolli, D. Bleiner, M. Groenewolt, S. Gross, Adv. Funct. Mater. 17 (2007) 1671.
[2] C.D. Pemmaraju, S. Sanvito, Phys. Rev. Lett. 94 (2004) 217205.
[3] G.D. Wilk, R.M. Wallace, J.M. Anthony, J. Appl. Phys. 89 (2001) 52443.
[4] S. Sayan, S. Aravamudhan, B.W. Busch, W.H. Schulte, F. Cosandey, G.D. wilk, T. Gustafsson, E. Garfunkel, J. Vac. Sci. Technol. A 20 (2002) 507.
[5] T. Nishide, S. Honda, M. Matsuura, M. Ide, Thin Solid Films 371 (2000) 61.
[6] S.J. Wang, P.C. Lim, A.C.H. Huan, C.L. Liu, J.W. Chai, S.Y. Chow, J.S. Pan, Q. Li, C.K. Ong, Appl. Phys. Lett. 82 (2003) 2047.
[7] K. Cherkaoui, S. Monaghan, M.A. Negara, M. Modreanu, P.K. Hurley, D.O. Connell, S. McDonnell, G. Hughes, S. Wright, R.C. Barklie, P. Bailey, T.C.Q. Noakes, J. Appl. Phys. 104 (2001) 064113.
[8] S. Bruns, M. VergÖhl, O. Werner, T. Wallendorf, Thin Solid Films 520 (2012) 4122.
[9] E.E. Hoppe, R.S. Sorbello, C.R. Aita, J. Appl. Phys. 101 (2007) 123534.
[10] J. Aarik, H. Mandar, M. Kirm, L. Pung, Thin Solid Films 466 (2004) 41.
[11] T. Ito, M. Maeda, K. Nakamura, H. Kato, Y. Ohki, J. Appl. Phys. 97 (2005) 054104.
[12] J. Ni, Q. Zhou, Z. Li, Z. Zhang, Appl. Phys. Lett. 93 (2008) 011905.
[13] V. Kiisk, S. Lange, K. Utt, T. Tätte, H. Mändar, I. Sildos, Physica B 405 (2010) 758.
[14] F. Biscarini, P. Samori, O. Greco, R. Zamboni, Phys. Rev. Lett. 78 (1997) 2389.
[15] H.J. Li, C.Y. Pu, C.Y. Ma, Sh. Li, W.J. Dong, S.Y. Bao, Q.Y. Zhang, Thin Solid Films 520 (2011) 212.
[16] K. Kamala Bharathi, N.R. Kalidindi, C.V. Ramana, J. Appl. Phys. 108 (2010) 083529.
[17] N.V. Nguyen, A.V. Davydov, D. Chandler-Horowitz, Appl. Phys. Lett. 87 (2005) 192903.
[18] A.A. Rastorguev, V.I. Belyi, T.P. Smirnova, L.V. Yakovkina, M.V. Zamoryanskaya, V.A. Gritsenko, H. Wong, Phys. Rev. B76 (2007) 235315.
[19] A. Ciapponi, F.R. Wagner, S. Palmier, J.Y. Natoli, L. Gallais, J. Lumin. 129 (2009) 1786.